Microwave Synthesis of an Aluminum Fluoride Hydrate with Cationic Vacancies: Structure, Thermal Stability, and Acidic Properties

Damien Dambournet,[†] Alain Demourgues,*[,†] Charlotte Martineau,[‡] Etienne Durand,[†] Jérôme Majimel,[†] Christophe Legein,[‡] Jean-Yves Buzaré,[§] Franck Fayon,[||,⊥] Alexandre Vimont,[#] Hervé Leclerc,[#] and Alain Tressaud[†]

Institut de Chimie de la Matière Condensée de Bordeaux-CNRS, Université Bordeaux 1, 87, Avenue du Dr. A. Schweitzer, 33608 Pessac cedex, France, Laboratoire des Oxydes et Fluorures, CNRS UMR 6010, and Laboratoire de Physique de l'Etat Condensé, CNRS UMR 6087, IRIM2F, CNRS FR 2575, Université du Maine, Avenue Olivier Messiaen, 72085 Le Mans Cedex 9, France, Conditions Extrêmes et Matériaux: Haute Température et Irradiation, UPR CNRS 3079, 1D Avenue de la Recherche Scientifique, 45071 Orléans Cedex 2, France, Faculté des Sciences, Université d'Orléans, Avenue du Parc Floral, 45067 Orléans Cedex 2, France, and Laboratoire Catalyse et Spectrochimie, UMR 6506, CNRS-ENSICAEN-Université de CAEN, Boulevard du Maréchal Juin, F-14050 Caen Cedex, France

Received September 1, 2008. Revised Manuscript Received September 18, 2008

Aluminum fluoride hydrate was synthesized by a microwave hydrothermal process. The structure derives from the ReO_3 type structure, that is, the high temperature structure of α-AlF_3. The cubic symmetry adopted by this compound arises from water molecules, stabilized as ligand surrounding Al^{3+} cations which induces cationic vacancies as revealed by Rietveld refinement. The following chemical formula $Al_{0.82}\square_{0.18}F_{2.46}(H_2O)_{0.54}$ is supported by chemical analysis and TGA measurements. This represents the first example of aluminum vacancy compound in the Al-based fluorides chemistry. High field ^{27}Al NMR spectroscopy enabled identification and quantification of the following species: AlF_6 and $AlF_{6-x}(H_2O)_x$ with $x = 1, 2, 3$, and showed that vacancies are mainly surrounded by water molecules but also by a low content of fluoride ions as also evidenced by ^{19}F NMR. The hydrogen bonding network, which takes place in the vicinity of the cationic vacancies, was characterized by FTIR and ^1H NMR spectroscopies. A 2:1 complex X···H−O−H···X where X is a proton acceptor, which is related to a shift of the $\nu_{sym}(OH)$ and $\nu_{asym}(OH)$, was detected. This complex appears to be stable up to 773 K. The phase transition into the rhombohedral form occurs at around 573 K, but at such a temperature a large amount of water molecules associated to cationic vacancies still remained thanks to the 2:1 complex. The acidic properties have been revealed by pyridine and CO probe molecules. At 573 K, the solid exhibits both strong Lewis and Brønsted acidities with an equivalent number of sites providing bifunctionality. The strong acidic behavior highlights the effect of water molecules/cationic vacancies on the surface structure. Whereas the Lewis strength acidity progressively decreases with dehydration, Brønsted acidity remains strong even at 773 K.

Introduction

The chemistry of the aluminum−fluorine system is very rich through the existence of several forms of AlF_3: α, β, η, θ, κ-AlF_3,[1] but for a long time these compounds could not be prepared as highly divided materials. The extreme reactivity of the fluorine element prevented the stabilization of nanoparticles using conventional "chimie douce" routes. Recently, microwave-assisted synthesis has allowed obtaining highly divided aluminum hydroxy-fluoride.[2,3] Tuning the OH/F molar ratio has been proved to be a decisive tool to get the required compositions and structures. Some aluminum fluorides are known to be strong Lewis acids.[4,5] The presence of OH groups in these materials enables the Brønsted/Lewis acidic behavior to be balanced. Water molecules can also be considered to act as potential strong Brønsted acid sites as revealed for instance in the case of alumino-silicates.[6] To be suitable for catalytic applications, anion species and

* To whom correspondence should be addressed. E-mail: demourg@icmcb-bordeaux.cnrs.fr.
† Université Bordeaux 1.
‡ Laboratoire des Oxydes et Fluorures, Université du Maine.
§ Laboratoire de Physique de l'Etat Condensé, Université du Maine.
|| UPR CNRS 3079.
⊥ Université d'Orléans.
CNRS-ENSICAEN-Université de CAEN.

(1) (a) Daniel, P.; Bulou, A.; Rousseau, M.; Nouet, J.; Fourquet, J.-L.; Leblanc, M.; Burriel, R. *J. Phys.: Condens. Matter* **1990**, *2*, 5663. (b) Fourquet, J.-L.; Rivière, M.; Le Bail, A. *Eur. J. Solid State Inorg. Chem.* **1988**, *25*, 535. (c) Le Bail, A.; Jacoboni, C.; Leblanc, M.; De Pape, R.; Duroy, H.; Fourquet, J.-L. *J. Solid State Chem.* **1988**, *77*, 96. (d) Herron, N.; Thorn, D. L.; Harlow, R. L.; Jones, G. A.; Parise, J. B.; Fernandez-Baca, J. A.; Vogt, T. *Chem. Mater.* **1995**, *7*, 75. (e) Le Bail, A.; Fourquet, J.-L.; Bentrup, U. *J. Solid State Chem.* **1992**, *199*, 151. (f) Ravez, J.; Mogus-Milankovic, A.; Chaminade, J.-P.; Hagenmuller, P. *Mater. Res. Bull.* **1984**, *19*, 1311.
(2) Dambournet, D.; Demourgues, A.; Martineau, C.; Pechev, S.; Lhoste, J.; Majimel, J.; Vimont, A.; Lavalley, J.-C.; Legein, C.; Buzaré, J.-Y.; Fayon, F.; Tressaud, A. *Chem. Mater.* **2008**, *20*, 1459.
(3) Dambournet, D.; Demourgues, A.; Martineau, C.; Durand, E.; Majimel, J.; Vimont, A.; Leclerc, H.; Lavalley, J.-C.; Daturi, M.; Legein, C.; Buzaré, J.-Y.; Fayon, F.; Tressaud, A. *J. Mater. Chem.* **2008**, *18*, 2483.
(4) Kemnitz, E.; Menz, D. H. *Prog. Solid State Chem.* **1998**, *26*, 97.
(5) Herron, N.; Farneth, W. E. *Adv. Mater.* **1996**, *12*, 8.

10.1021/cm8023617 CCC: $40.75
Published on Web 10/29/2008

water should be thermally stable. The occurrence of both acidities can be suitable for peculiar reactions involving a Brønsted/Lewis acid synergy, as reported for instance in zeolite-promoted hydrocarbons reactions.[7] Such a synergetic effect has been evidenced by ab initio calculations to occur with HF and AlF_3. The synergy between both catalysts enables a drastic lowering of the activation barrier of the formamide synthesis.[8]

Aluminum fluoride hydrates have been used as precursors to prepare various forms of AlF_3. For instance, the decompositions of α- and β-$AlF_3 \cdot 3H_2O$ that occur at rather low temperatures (<623 K) lead to the metastable β-AlF_3 form and the thermodynamically stable one α-AlF_3, respectively.[4] The most known among the aluminum fluoride hydrates, that is, $AlF_3 \cdot 9H_2O$ and α- and β-$AlF_3 \cdot 3H_2O$, have been recently reinvestigated using X-ray/neutron diffractions and nuclear magnetic resonance (NMR) spectroscopy.[9] These structures are built either from isolated octahedra for the first two compounds ($AlF_3 \cdot 9H_2O$, α-$AlF_3 \cdot 3H_2O$) or 1D chains of corner-bridging $AlF_{6-x}(H_2O)_x$ octahedra for the third one (β-$AlF_3 \cdot 3H_2O$) with the hydrogen network giving rise to a low thermal stability.

The α-form of aluminum trifluoride has received extended attention over the years. This structure adopts a distorted ReO_3-type structure and undergoes a first-order phase transition at around 723 K into the cubic ReO_3 form.[1a] The phase transition has been studied using molecular dynamics simulations, and the anion polarization has been established as the driving force of the tilting AlF_6 octahedra.[10] Fluorination of γ-Al_2O_3 with $CHClF_2$ led to a catalytically active phase[11] which has been identified as the cubic α-AlF_3 form, highlighting potential application as catalyst. Concomitantly, ab initio calculations performed on the (0001) surface of the rhombohedral form of α-AlF_3 show that potential Lewis acid sites are masked by two fluoride ions leading to poor Lewis acidity.[12,13] However, Lewis acid centers have been evidenced to occur on a clean α-AlF_3 $(01\bar{1}2)$ surface.[14] Nevertheless, the conditions to avoid hydroxylation which provokes the inaccessibility of these centers have been concluded to be unrealistic.[14] Additionally, molecular dynamic simulation performed on cubic α-AlF_3 nanoparticles showed the occurrence of potential strong Lewis acid sites.[15] The rhombohedral form α-AlF_3 therefore appears as a weak Lewis catalyst whereas a small perturbation of the network, that is, cubic symmetry, seems to lead to a completely different surface structure generating Lewis acidity.

The present work reports the synthesis and the characterization of a new aluminum fluoride hydrate exhibiting the ReO_3-type structure. Powder Rietveld refinement, high resolution transmission electron microscopy (HRTEM), BET measurement, ^1H, ^{19}F and ^{27}Al magic angle spinning (MAS) NMR investigations, thermogravimetric analysis coupled with mass spectrometry (TGA-MS), and Fourier transform infrared (FTIR) analysis with and without the adsorption of probe molecules (pyridine, CO) have been used to characterize the structural features and acidic properties of this compound.

Experimental Procedures

1. Synthesis Procedure. Synthesis was performed using a MARS-5 Microwave Digestion System oven (CEM Corp.). A precursor solution was first prepared as follows: 25 mmol of Al(III) chloride hexahydrated ($AlCl_3 \cdot 6H_2O$, Sigma-Aldrich: 99%) was added to a solution containing 10 mL of isopropanol (Isopropanol Sigma-Aldrich 98%) and 10 mL of distilled water. An aqueous HF solution (Panreac 40%) was added to the mixture in proportions ensuring an [HF]/[Al] molar ratio equal to 3.5. The solution was placed in a closed Teflon container (XP-1500 plus model) and submitted to microwave heating for 1 h to a temperature of 413 K (17 K min^{-1}). After microwave-assisted drying performed for 30 min under primary vacuum and argon flow at 373 K a powdered sample was recovered. The sample was washed with a large amount of ethanol under nitrogen flow. No retention of ethanol or ethoxide formation have been detected.

2. Characterizations. *Elemental Analysis.* The final [F]/[Al] molar ratio was measured by electron probe microanalysis (EPMA) using a Castaing microprobe CECAMA SX 630 apparatus equipped with wavelength dispersive spectrometry. The [F]/[Al] molar ratio is given with error bars equal to 0.05.

X-ray Diffraction Analysis. The compounds were characterized by X-ray powder diffraction (XRPD) using a Philips PW 1050 diffractometer in a Bragg−Brentano geometry with Cu Kα radiation ($K\alpha_1 = 1.54059$ Å and $K\alpha_2 = 1.54441$ Å). The intensity data were collected at room temperature over a 2θ range of 5−110° with 0.02° steps and an integration time of 10 s. The whole pattern profile matching and the Rietveld structural refinement were performed with the FULLPROF program.[16]

Surface Area Measurement. Prior to adsorption, around 200 mg of the powdered sample were evacuated overnight at 573 K under 0.1 Pa. N_2 adsorption isotherms were performed at 77 K using an ASAP 2000 instrument from Micromeritics. The specific surface area S_{BET} was calculated from BET results applied in the P/P^0 [0.03−0.25] range.

Transmission Electron Microscopy. Transmission electron microscopy (TEM) was performed on a TECNAI F20 equipment with a field emissive gun (operating at 200 kV and with a point resolution of 0.24 nm). The Gatan Digital Micrograph software was used to calculate the fast Fourier transforms (FFT) of HRTEM. TEM samples were prepared by dissolving a few milligrams of powder in ethanol. The solution was then dipped for 10 min into an ultrasonic bath so as to disagglomerate the powder particles. One drop of the solution was finally deposited on a Formvar/carbon copper grid.

(6) Garrone, E.; Onida, B.; Bonelli, B.; Busco, C.; Ugliengo, P. *J. Phys. Chem. B* **2006**, *110*, 19087.
(7) Li, S.; Zheng, A.; Su, Y.; Zhang, H.; Chen, L.; Yang, J.; Ye, C.; Deng, F. *J. Am. Chem. Soc.* **2007**, *129*, 11171.
(8) Rimola, A.; Tosoni, S.; Sodupe, M.; Ugliengo, P. *Chem. Phys. Lett.* **2005**, *408*, 295.
(9) Kemnitz, E.; Gross, U.; Rüdiger, St.; Scholz, G.; Heidemann, D.; Troyanov, S. I.; Morosov, I. V.; Lemée-Cailleau, M.-H. *Solid State Sci.* **2006**, *8*, 1443.
(10) Chaudhuri, S.; Chupas, P. J.; Wilson, M.; Madden, P.; Grey, C. P. *J. Phys. Chem. B* **2004**, *108*, 3437.
(11) Chupas, P. J.; Ciraolo, M. F.; Hanson, J. C.; Grey, C. P. *J. Am. Chem. Soc.* **2001**, *123*, 1694.
(12) Wander, A.; Searle, B. G.; Bailey, C. L.; Harrison, N. M. *J. Phys. Chem. B* **2005**, *109*, 22935.
(13) Wander, A.; Bailey, C. L.; Mukhopadhyay, S.; Searle, B. G.; Harrison, N. M. *J. Mater. Chem.* **2006**, *16*, 1906–1910.
(14) Mukhopadhyay, S.; Bailey, C. L.; Wander, A.; Searle, B. G.; Muryn, C. A.; Schroeder, S. L. M.; Lindsay, R.; Weiher, N.; Harrison, N. M. *Surf. Sci.* **2007**, *601*, 4433.
(15) Chaudhuri, S.; Chupas, P.; Morgan, B. J.; Madden, P. A.; Grey, C. P. *Phys. Chem. Chem. Phys.* **2006**, *8*, 5045.
(16) Rodríguez-Carvajal, J. *Physica B.* **1993**, *192*, 55.

FTIR Spectroscopy. Infrared transmission spectra were recorded on self-supporting wafers (2 cm^2, 20 mg) which were placed into an infrared quartz cell (KBr windows) connected to a vacuum line. Samples were activated under vacuum at 573 K overnight. Spectra were recorded with a resolution of 4 cm^{-1}. The IR spectrometer was a Nicolet Nexus apparatus equipped with an extended KBr beam splitter and a mercury cadmium telluride (MCT) detector. Probe molecules were introduced into the cell via the vacuum line. After activation, the acidity of the materials was studied using adsorption of pyridine and CO (at 100 K).

NMR Spectroscopy. The ^{19}F and ^{1}H Hahn echo Magic Angle Spinning (MAS) NMR spectra were acquired on an Avance 300 Bruker spectrometer ($B_0 = 7$ T), using a 2.5 mm ^{19}F optimized CP MAS probe, operating at a Larmor frequency of 282.2 and 300.1 MHz for ^{19}F and ^{1}H, respectively. The 90° pulse durations were set to 4 μs (RF field 60 kHz) and 2.5 μs (RF field 100 kHz) for ^{19}F and ^{1}H, respectively, with an interpulse delay equal to one rotor period. The recycle delays were taken to 10 and 1 s for ^{19}F and ^{1}H, respectively. The ^{19}F chemical shifts were referenced to $CFCl_3$ at 0 ppm. The ^{1}H chemical shifts were referenced to ^{1}H in TMS at 0 ppm. These spectra were reconstructed using DMFIT software.[17]

The ^{27}Al ($I = 5/2$) MAS NMR spectrum was recorded using a 2.5 mm CP MAS probe on an Avance 750 Bruker spectrometer ($B_0 = 17.6$ T) and an Avance 300 Bruker spectrometer ($B_0 = 7$ T) operating at a ^{27}Al Larmor frequency of 195.5 and 78.2 MHz, respectively. A short pulse length of 1 μs was used to ensure quantitative excitation of the whole spin system. The recycle delay was set to 1 s. ^{27}Al spectra were referenced to 1 M aqueous solution of $Al(NO_3)_3$. Quantitative reconstructions[18−21] of the main resonance of the ^{27}Al NMR spectra were achieved taking into account the $N = 0$ spinning sideband of the satellite transitions $\langle 3/2 \rangle$ and the $N = 0$ spinning sideband of the central transition $\langle 1/2 \rangle$ which completely overlap. For each ^{27}Al NMR site, the isotropic chemical shift δ_{iso} and the quadrupolar product $\nu_{Q\eta}$ were calculated by comparison of the center of gravity $\delta_{cs}^{\langle 3/2 \rangle}$ of the Al satellite sideband with that of the central transition $\delta_{cs}^{\langle 1/2 \rangle}$, through the following equation:

$$\delta_{cs}^{\langle m \rangle} = \delta_{iso} - \nu_{Q\eta}^2 \frac{[I(I+1) - 3 - 9m(m-1)]}{30\nu_0^2} \times 10^6$$

where $I = 5/2$ in the case of ^{27}Al, $\nu_0 = 195.5$ MHz (for the 17.6 T spectrometer), and $\nu_{Q\eta} = \nu_Q[1 + (\eta_Q^2/3)]^{1/2}$.[20] A two-dimensional one pulse[22−24] (TOP) spectrum was constructed by stacking subspectra shifted by the spinning frequency from the 1D MAS NMR spectra.

Thermogravimetric Analysis. The thermal behavior was studied by simultaneously coupled TA-MS measurements. A NETZSCH thermoanalyzer STA 409 C, equipped with a BALZERS QMG 421, was used to record the thermoanalytical curves (T, DTA, TG, DTG) together with the ionic current (IC) curves in the multiple ion detection (MID) mode. A constant purge gas flow of 70 mL/min nitrogen (MESSER-GRIESHEIM 5.0) and a constant heating rate of 10 K/min were applied.

Results and Discussion

1. Microwave-Assisted Synthesis and Determination of the Chemical Composition. Microwave-assisted synthesis was recently proved to be an efficient way to obtain nanosized crystallized aluminum fluorides. This method enables the achievement of high surface area aluminum hydroxyfluorides exhibiting either the pyrochlore-type[3] (137 $m^2 \cdot g^{-1}$) or the metastable hexagonal tungsten bronze-type which is alternatively named β or HTB(82 m^2/g)[2]. During these investigations, it has been demonstrated that some key parameters play a decisive role in the stabilization of the final structure and in getting high surface area materials. Among them, the $R = [HF]/[Al]$ molar ratio was proved to be a relevant parameter in the stabilization of the final form. Using nitrate ($Al(NO_3)_3$) as aluminum precursor, three domains could be distinguished: $R = 2$, $R = 3$, and $R > 3$. For $R = 2$ and $R = 3$, the pyrochlore-type structure and a derived form of β-AlF_3 were obtained, respectively. Higher [HF] contents, that is, $R > 3$, led to a mixture containing β-AlF_3, rhombohedral and cubic forms of Al-based fluoride. The influence of the aluminum precursor on the stabilized structures was also found to be decisive. For $R = 3$, aluminum chloride as precursor led to a mixture of β-AlF_3 and α-AlF_3, whereas Al nitrate, by being reduced into ammonium ions during the microwave-assisted synthesis, enabled the stabilization of the metastable phase β-AlF_3.

Chloride precursor, however, appears interesting when a solution with high [HF]/[Al] molar ratio is added to a water/isopropanol mixture. The hydrothermal microwave heat treatment of the resulting mixture enables a powder which can be indexed with the ICDD-JSPDS file No. 72-1117 be prepared, referred as $AlF_3 \cdot H_2O$. It should be noted that the procedure should be carefully followed to get phase purity. The structure of this material was solved by Chandross[25] using a cubic lattice ($Pm\bar{3}m$) and a unit cell parameter, $a = 3.610$ Å, which is closely related to that of the high temperature phase[11] of the thermodynamically stable phase α-AlF_3 ($R\bar{3}c$). In this paper, the water molecules were located in the center of the cube with AlF_6 octahedra at the corners. Nevertheless, the poor agreement factor reported by the author, that is, 16.4%, revealed an unrealistic structural model. In such conditions, we decided to reinvestigate the structure of this material, as it will be described in the next section.

The chemical composition of the compound was determined prior to the structure investigation. EPMA gave a F/Al molar ratio equal to 3.00(5). The occurrence of a very small amount of OH groups cannot be excluded. Thermogravimetric analysis coupled with a mass spectrometer was performed up to 1073 K, and a weight loss of 13.8% was measured. The weight loss was mainly ascribed to the release of water through the ionic curve $m/z = 18$, characterizing

(17) Massiot, D.; Fayon, F.; Capron, M.; King, I.; Le Calvé, S.; Alonso, B.; Durand, J.-O.; Bujoli, B.; Gan, Z.; Hoatson, G. *Magn. Reson. Chem.* **2002**, *40*, 70.
(18) Massiot, D.; Bessada, C.; Coutures, J. P.; Taulelle, F. *J. Magn. Reson.* **1990**, *90*, 231.
(19) Alemany, L. B.; Massiot, D.; Sherriff, B. L.; Smith, M. E.; Taulelle, F. *Chem. Phys. Lett.* **1991**, *177*, 301.
(20) Massiot, D.; Müller, D.; Hübert, Th.; Schneider, M.; Kentgens, A. P. M.; Coté, B.; Coutures, J. P.; Gessner, W. *Solid State Nucl. Magn. Reson.* **1995**, *5*, 175.
(21) Stebbins, J. F.; Kroeker, S.; Lee, S. K.; Kiczenski, T. J. *J. Non-Cryst. Solids* **2000**, *275*, 1–6.
(22) Blümich, B.; Blumler, P.; Jansen, J. *Solid State Nucl. Magn. Reson.* **1992**, *1*, 111.
(23) Blumler, P.; Blümich, B.; Jansen, J. *Solid State Nucl. Magn. Reson.* **1994**, *3*, 237.
(24) Massiot, D.; Hiet, J.; Pellerin, N.; Fayon, F.; Deschamps, M.; Steuernagel, S.; Grandinetti, P. J. *J. Magn. Reson.* **2006**, *181*, 310.
(25) Chandross, R. *Acta Crystallogr.* **1964**, *17*, 1477.

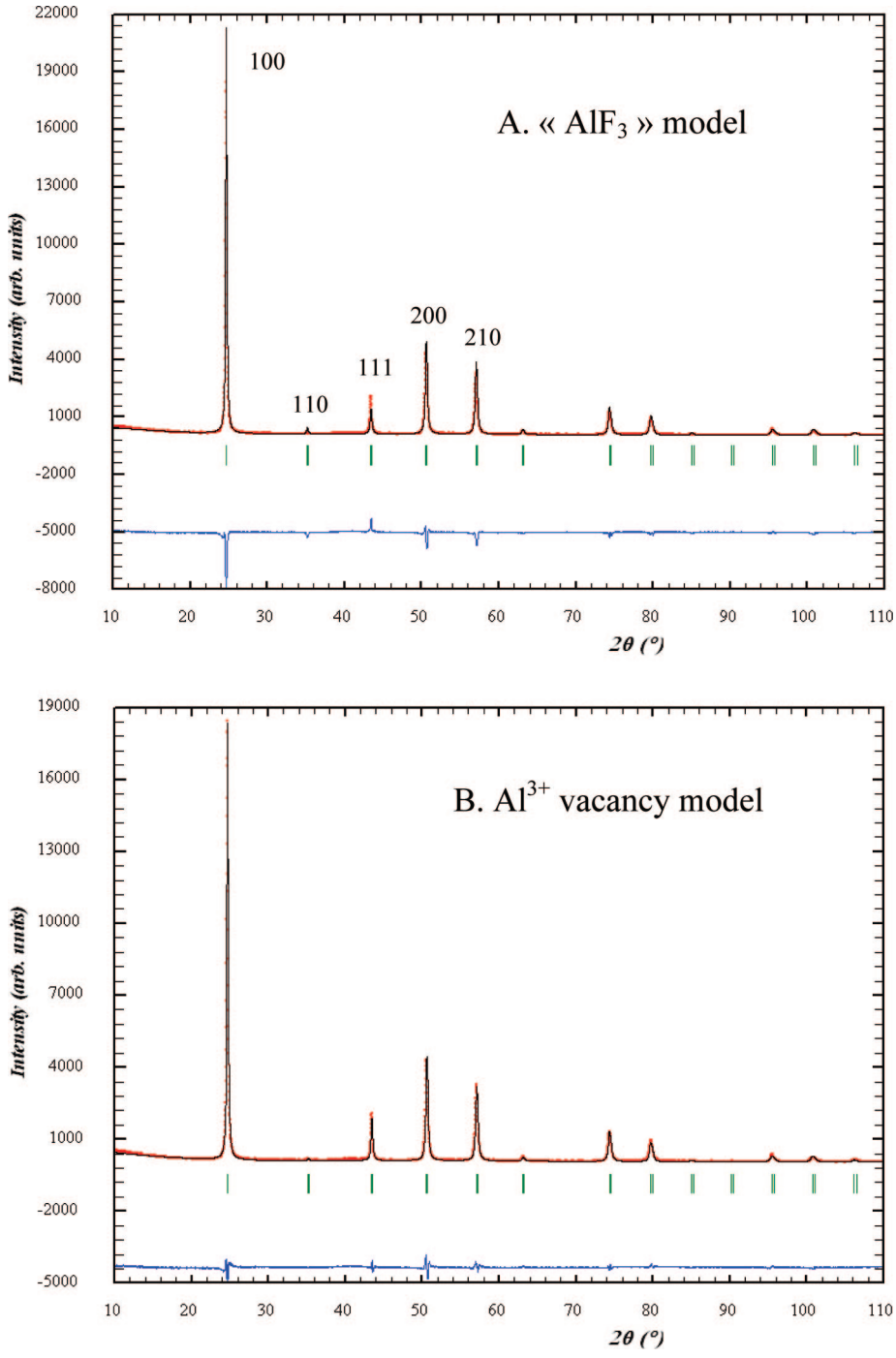

Figure 1. Rietveld plot obtained using (A) α-AlF_3 cubic model and (B) model with cation vacancies. Experimental X-ray diffraction powder pattern (red curve) compared to the Rietveld refined profile (black curve) and the difference curve (blue curve). The vertical bars correspond to the positions of the Bragg reflections.

H_2O^+ fragments. However, a low signal corresponding to F ($m = 19$) on the mass spectrometer has been identified starting from $T = 773$ K. The presence of structural water was further confirmed by FTIR spectroscopy, as it will be discussed later. When aged in moist air, the material undergoes a partial decomposition with the detection by XRD of traces of the pyrochlore phase.

2. Structural Investigation. *2.1. Rietveld Refinement.* Rietveld refinement was first performed using the high temperature α-AlF_3 structure ($Pm\bar{3}m$, $a = 3.60$ Å),[11] where Al^{3+} ions are placed at the corner of the cube (0, 0, 0), and F^- ions on the edge (1/2, 0, 0). A poor agreement factor $R_{Bragg} = 18.8\%$ was obtained for such a model (Figure 1A). In a first step, the presence of water on the center (1/2, 1/2, 1/2) of the cube was tested; however, no residual electron density at this atomic position has been found, and the Bragg factor remains high around 18%. In a second step, we introduced a water molecule in the first coordination sphere of the Al^{3+} ions. The resulting octahedra element can then be written as $[AlF_{6-x}(H_2O)_x]^{x-3}$, in which water is considered as neutral; the lack of electron density upon the octahedra should be balanced by the occurrence of cation vacancies. Rietveld refinement was therefore performed based on this new structural model where the cation

Table 1. X-ray Refinement Data

crystal symmetry: cubic

space group: $Pm\bar{3}m$; $Z = 1$

atom (Wyckoff position)	x, y, z	B_{iso} (Å^2)	occupancy	reliability factor (%)
	A. "AlF_3" model			
Al^{3+} (1a)	0,0,0	0.7(3)	1	χ^2: 7.37
F^- (3d)	1/2,0,0	2.1(5)	1	cR_p: 27.5
				cR_{wp}: 26.6
				R_{Bragg}: 18.8
	B. Al^{3+} vacancies model			
Al^{3+} (1a)	0,0,0	0.6(3)	0.816(18)	χ^2: 3.37
F^- (3d)	1/2,0,0	2.1(4)	0.820(6)	cR_p: 17.8
H_2O (3d)	1/2,0,0	2.1(4)	0.178(6)	cR_{wp}: 18.0
				R_{Bragg}: 4.3

$a = 3.6067(1)$ Å
Al−F: 1.8034(1) Å
F−F: 2.5503(1) Å

vacancies are correlated with the occurrence of H_2O molecules substituting F^- ions. The anionic site (3a) is statistically occupied either by F^- ions or H_2O molecules (Table 1). A relation which can be summarized by the chemical formula $Al_{1-x}\square_xF_{3-3x}(H_2O)_{3x}$was used in the Rietveld refinement to ensure the electroneutrality of the model. The corresponding model strongly improved the Rietveld refinement to a better agreement factor R_{Bragg} equal to 4.3% (Figure 1B). One should notice the disorder for the F/H_2O site revealed by the high Debye−Weller factor (Table 1). This disorder can be explained by the occupancy of the same crystallographic site by F^- ions and H_2O molecules and the occurrence of Al^{3+} vacancies. Table 1 summarizes the refinement results obtained using the stoichiometric either or Al^{3+} vacancy models.

On the basis of the refinement and chemical analysis, the corresponding formula could be established: $Al_{0.82}\square_{0.18}F_{2.46}(H_2O)_{0.54}$. This represents the first example of aluminum vacancy compound in the Al-based fluoride chemistry. Several density measurements have been performed, but because of the water departure, these data are not exploitable. Thermogravimetric analysis was in rather fair agreement with the above chemical formula, that is, the experimental weight loss deduced from thermogravimetric analysis is equal to 13.8% versus 12.4% calculated from Rietveld refinement with the above formula. The difference can arise from standard deviation from Rietveld refinement and/or from the release of HF molecules resulting from the reaction of water with the fluoride network. One should note that a low signal corresponding to F($m = 19$) is detected on mass spectrometer starting from $T = 773$ K.

The cubic symmetry of the structure was confirmed by the fast Fourier transforms (FFT) of HRTEM images displayed in Figure 2 (inset). It can be noted that the cubic symmetry is additionally reflected by the shape of the particles (Figure 2).

X-ray diffraction line broadening analysis was used to get more insight into the microstructure with the calculation of the microstrains ($\Delta d/d$) and crystallite size. By using the global profile refinement, the microstructural features (coherent domains and microstrains) were extracted from the additional line broadening of the Bragg peaks. Instrumental contribution was established by the XRD pattern of standard LaB_6 powder. Isotropic contributions were considered for both coherent domains and microstrains. The calculated average size particle is 50 nm, which is in agreement with HRTEM observation (Figure 2), and the calculated microstrains value is $\Delta d/d = 2 \times 10^{-3}$. It should be noted that some microdistortions have been observed on HRTEM images confirming the results of XRD analysis. The occurrence of water molecules inside the network could be at the origin of such a microdistorsion.

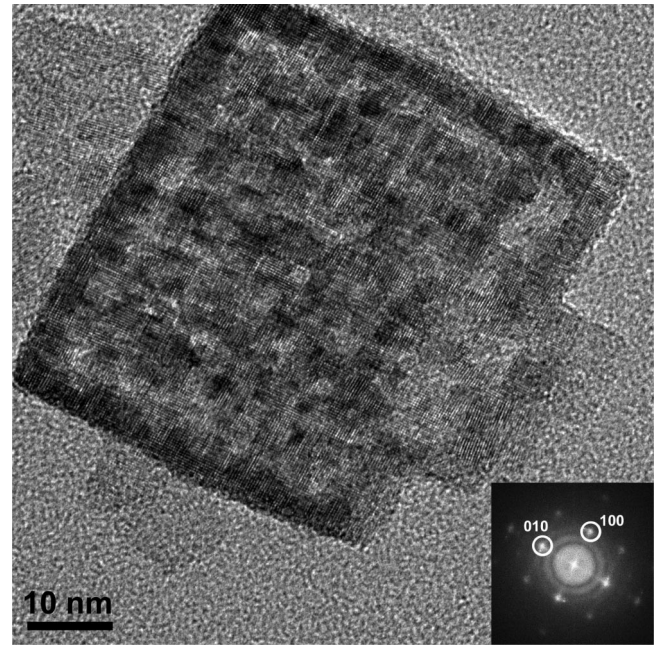

Figure 2. HRTEM micrograph of a particle of cubic aluminum fluoride hydrate. Inset: digital diffractogram of the nanoparticle revealing a [001] zone axis.

2.2. Evolution of the Structural Features upon Annealing. As previously mentioned, during the TG analysis the thermodesorption process of water has been followed using mass spectrometry (Figure 3). The ionic curve $m/z = 18$ (H_2O^+) shows three events located at 413, 563, and 588 K. The first one can be ascribed to the departure of water molecules. The second event is very weak and can be ascribed to structural water which appears less stable than those for which the departure occurs at 588 K. This last one is very intense but seems thereafter to continue over a large range of temperatures, that is, up to 973 K. It should be noted that a weak endothermic effect concomitant with the third event is detected on the DTA curve close to 588 K.

The effect of the dehydration upon the structure has been studied by annealing $Al_{0.82}\square_{0.18}F_{2.46}(H_2O)_{0.54}$ at various temperatures, that is, from 373 to 773 K. Samples were annealed under Ar flow (10 mL·min^{-1}) for 24 h. The corresponding room temperature powder XRD patterns of annealed samples are displayed in Figure 4. The cubic form appears to be stable up to 473 K with a smaller unit-cell constant probably associated to water departure and the reduction of cation vacancy rate. After annealing at higher temperatures, some X-ray diffraction lines split, revealing a lower symmetry. At 573 K, the cubic phase undergoes a rhombohedral distortion which is associated

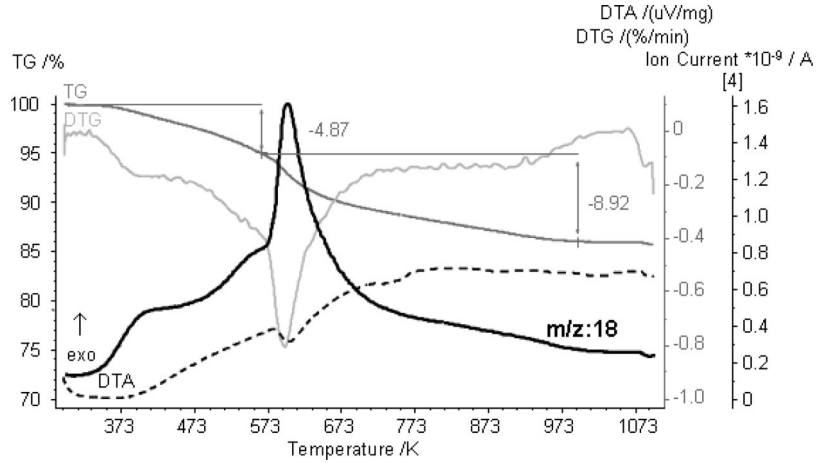

Figure 3. Thermogravimetric (DTG, DTA) analyses and mass spectrometry curve of $m/z = 18$ (H_2O^+ fragment) performed on the cubic aluminum fluoride hydrate.

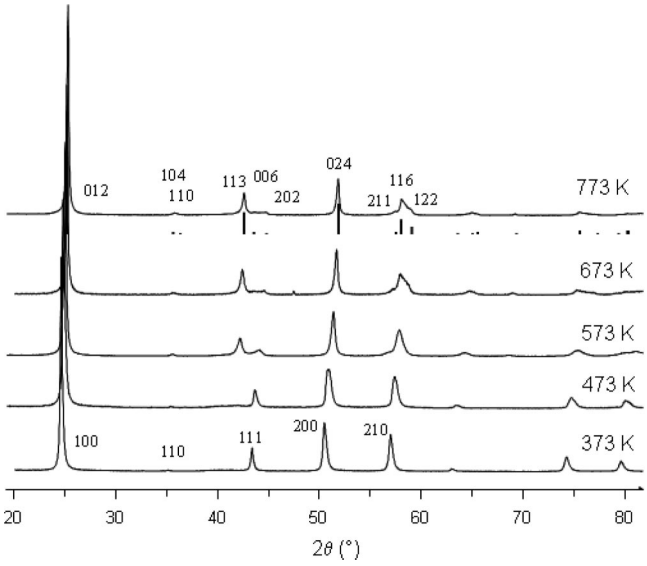

Figure 4. Evolution of the powder XRD patterns (room temperature) of cubic aluminum fluoride hydrate after annealing at various temperatures. Vertical bars represent the XRD peaks positions of α-AlF_3 ($R\bar{3}c$) from ICDD-JCPDS file No. 44-0231.

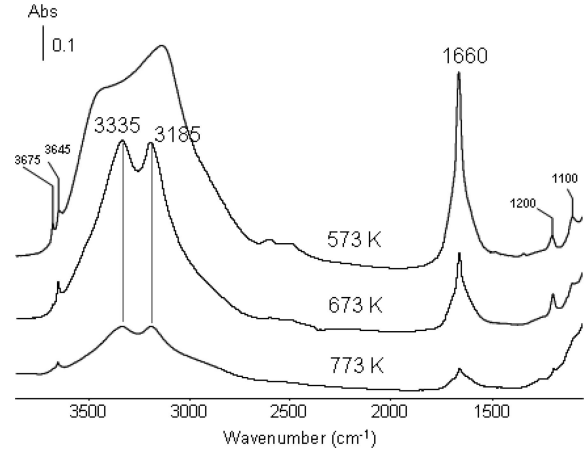

Figure 5. IR spectra of cubic aluminum fluoride hydrate recorded after in situ annealing at various temperatures.

in the DTA curve with the small endothermic phenomenon. The Bragg peaks corresponding to the rhombohedral form of α-AlF_3 have been included in Figure 4, accounting for the symmetry change.

2.3. Hydrogen Bonding Network Characterization. FTIR spectroscopy has been further used to study the stability of water molecules. Additionally, this technique enables the conformation of water molecules to be probed and the occurrence of hydrogen bonding inside the structure to be checked. The interanionic distance obtained from Rietveld refinement is 2.55 Å, a value which should lead to strong hydrogen bonding.[26,27] Due to the large amount of water in the sample, the IR spectrum presents a high signal-to-noise ratio. For sake of clarity, the sample was annealed in situ at various temperatures up to 773 K to reduce such a background. IR spectra of $Al_{0.82}\square_{0.18}F_{2.46}(H_2O)_{0.54}$ after annealing at 573, 673, and 773 K are displayed in Figure 5. The spectra reveal two types of contributions located in the 2800−3700 cm^{-1} and 1600−1700 cm^{-1} ranges which are ascribed to the stretching and deformation modes of water molecules, respectively. The large envelop detected in the 2800−3700 cm^{-1} range confirms the occurrence of hydrogen bonding inside the structure. The stability of structural water molecules is clearly evidenced since the stretching and deformation modes of H_2O are still detected at 773 K. The two contributions decrease significantly during the annealing process. At 573 K, in the 2800−3500 cm^{-1} region (water molecules linked by hydrogen bonding), two bands can be clearly distinguished at 3185 and 3335 cm^{-1}.

Without any interaction, the water molecule is built of "free OH bonds" which exhibit two OH stretching modes, ν_{sym}(OH) and ν_{asym}(OH) vibrating at 3616 and 3708 cm^{-1}, respectively.[28] The shifts of these two frequencies depend on the energy of the hydrogen bonding interaction, that is, the stronger the hydrogen bonding, the larger the shift toward low wavenumbers.[28] The position of the two perturbed ν(OH) thus accounts for moderate hydrogen bonding. The shift from the "free OH bond" is almost similar for both

(26) Jeffrey, G. A. *An Introduction to Hydrogen Bonding*; Oxford University Press: Oxford, 1997.
(27) Steiner, T. *Angew. Chem., Int. Ed.* **2002**, *41*, 48.
(28) Scatena, L. F.; Brown, M. G.; Richmond, G. L. *Science* **2001**, *292*, 908.

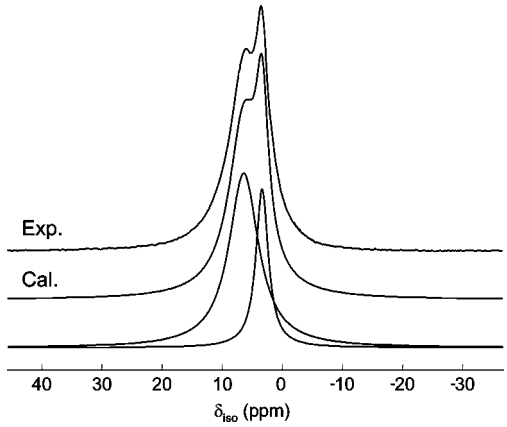

Figure 6. Experimental and calculated ^{1}H MAS (30 kHz) NMR spectra of $Al_{0.82}\square_{0.18}F_{2.46}(H_2O)_{0.54}$. The two individual contributions to the reconstructed spectrum are shown.

Table 2. Isotropic Chemical Shift δ_{iso} (ppm), Line Width (ppm), and Relative Intensity (%) As Deduced from the Reconstruction of the ^{1}H NMR Spectrum of $Al_{0.82}\square_{0.18}F_{2.46}(H_2O)_{0.54}$

line	δ_{iso} (±0.2)	width (±0.2)	intensity (±1)
1	5.0	2.5	27
2	8.0	6.0	73

ν_{sym}(OH) and ν_{asym}(OH) suggesting similar hydrogen bonding strength interactions. The corresponding complex is called a 2:1 complex[29] and can be written as X···H−O−H···X where X is a proton acceptor (X = F^-, OH^-). Water molecules can act as both hydrogen donor and hydrogen acceptor with F^- ions and neighboring water molecules, respectively. A complex hydrogen network is therefore assumed to occur.

Additionally, the deformation mode of water molecules $\delta(H_2O)$ is detected at 1660 cm^{-1} which corresponds to a shift of 60 cm^{-1} as compared to water in an inert solvent and accounts for water molecules involved in hydrogen bonding,[30,31] confirming the above observations. Some very weak bands which can be ascribed to hydroxyl groups are also detected. Such bands are indeed observed at 1100−1200 and 3645−3675 cm^{-1} (Figure 5) and may account for the deformation and stretching mode of hydroxyl groups,[32] respectively. Traces of hydroxyl groups can thus be considered, even at high temperatures.

^{1}H solid-state NMR was used to confirm the existence and the strength of hydrogen bonds in the hydrate form. Two ^{1}H resonances with δ_{iso} = 5.0 and 8.0 ppm are readily apparent in the ^{1}H MAS NMR spectrum of $Al_{0.82}\square_{0.18}F_{2.46}(H_2O)_{0.54}$ (Figure 6 and Table 2). The proton is increasingly deshielded with increasing hydrogen bond strength, which leads to ^{1}H downfield shifts. The two resonances can then be assigned to non- or weak H-bonded and moderate H-bonded[26,27] protons, respectively. ^{1}H downfield shifts can be correlated with the length of the hydrogen bond.[26,33] It has been shown that ^{1}H chemical shifts of oxygen-bonded hydrogen linearly depend on the O−H···O distance, through the following relation:

$$d(\mathrm{O}\cdots\mathrm{O})\ (\mathrm{pm}) = \frac{79.05 - \delta_{iso}\ (\mathrm{ppm})}{0.255}$$

d(O···O) (pm) = (79.05 − δ_{iso}(ppm))/0.255.[33] This relation allows an estimation of the O···O distance for H_2O molecules involving H-bonded hydrogen atoms, that is, 2.79 Å. The O···O distance estimated from this empirical relation and experimental ^{1}H isotropic chemical shift is typical of hydrogen bonds with water molecules (mean O···O distance equal to 2.825 Å)[27] and is significantly larger than the O/F···O/F distance determined by Rietveld analysis (2.55 Å, Table 1), indicating that H_2O molecules are only in average located on the 3d sites, in agreement with the disorder outlined above for the F/H_2O site. Finally, from both ^{1}H NMR and IR studies, hydrogen bonds appear moderate in $Al_{0.82}\square_{0.18}F_{2.46}(H_2O)_{0.54}$ following the classification of Jeffrey.[26]

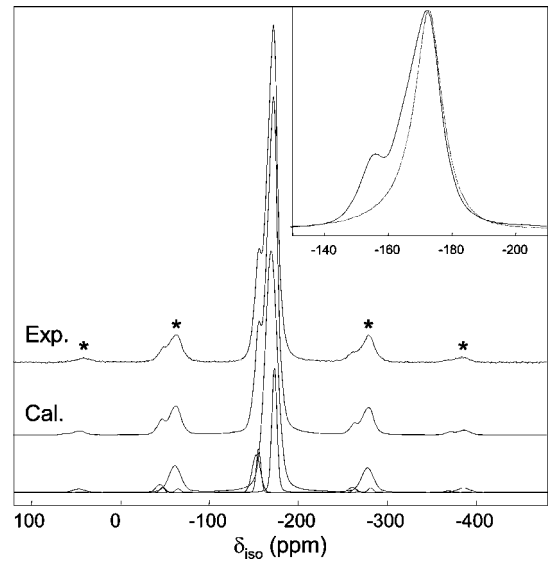

Figure 7. Experimental and calculated ^{19}F MAS (30 kHz) NMR spectra of $Al_{0.82}\square_{0.18}F_{2.46}(H_2O)_{0.54}$. The star symbols indicate the spinning sidebands. The four individual contributions to the reconstructed spectrum are shown. Experimental ^{19}F MAS (30 kHz) NMR spectra of $Al_{0.82}\square_{0.18}F_{2.46}(H_2O)_{0.54}$ and compound obtained after annealed at 773 K during 24 h under Ar (dash line) are presented in the inset.

The ^{1}H MAS NMR spectrum of the sample annealed at 773 K (shown in Supporting Information) exhibits a single broad resonance at 5.0 ppm in agreement with the disappearance of the hydrogen bond network, supported by IR study showing the occurrence of residual H_2O molecules in the sample annealed at 773 K.

2.4. Local Environments of Al^{3+} and F^- Ions: Influence of Cationic Vacancies and H_2O Molecules. ^{19}F and ^{27}Al high field solid-state NMR was used to probe the local environments of F^- and Al^{3+} ions. Two compounds have been considered, that is, the hydrate form and the compound annealed at 773 K.

^{19}F MAS NMR spectra of the hydrate form and the annealed compound are displayed in Figure 7. The hydrate compound spectrum shows two major contributions reconstructed using four signals (Table 3). The lowest δ_{iso} value (line 1, −173 ppm) may be related to bridging fluorine atoms

(29) Bricknell, B. C.; Ford, T. A.; Letcher, T. M. *Spectrochim. Acta, Part A* **1997**, *53*, 299.
(30) Burneau, A. *J. Mol. Liq.* **1990**, *46*, 99.
(31) Burneau, A.; Corset, J. *J. Chim. Phys.* **1972**, *69*, 171.
(32) Vimont, A.; Lavalley, J. C.; Francke, L.; Demourgues, A.; Tressaud, A.; Daturi, M. *J. Phys. Chem. B* **2004**, *108*, 3246.
(33) Eckert, H.; Yesinowski, J. P.; Silver, L. A.; Stolper, E. M. *J. Phys. Chem.* **1988**, *92*, 2055.

Table 3. Isotropic Chemical Shifts δ_{iso} (ppm), Line Widths (ppm), and Relative Intensities (%) As Deduced from the Reconstruction of the ^{19}F NMR Spectrum of $Al_{0.82}\square_{0.18}F_{2.46}(H_2O)_{0.54}$

line	δ_{iso} (±0.5)	width (±0.5)	intensity (±0.5)
1	−173.0	6.7	13.4
2	−169.4	16.0	74.3
3	−155.2	6.1	4.4
4	−152.5	11.0	7.9

in AlF_6 octahedra (δ_{iso} (^{19}F in α- and β-AlF_3) = −172 ppm[11]). ^{19}F chemical shifts of octahedral aluminum environments with oxygen and fluorine in the first coordination sphere increase with the oxygen content.[2,3,9,11,34−40] The isotropic chemical shift of line 2 is similar to those observed in aluminum hydroxy-fluoride derived from β-AlF_3[2] and pyrochlore[3] without cationic vacancy. So from its isotropic chemical shift, line 2 can be assigned to bridging fluorine atoms in $AlF_{6-x}(H_2O)_x$ octahedra with $x \geq 1$. Nevertheless, line 2 being broad, the lowest chemical shifts of this line may also contain contributions from bridging fluorine atoms in AlF_6 octahedra. Lines 3 and 4, at higher isotropic chemical shifts, are attributed to nonbridging fluorine atoms in $AlF_{6-x}(H_2O)_x$ octahedra, that is, fluorine atoms between an aluminum atom and a vacancy. This is in agreement with chemical shift values observed in aluminum fluoride hydrate built from isolated aluminum octahedra, $AlF_3 \cdot 9H_2O$ and α-$AlF_3 \cdot 3H_2O$ (δ_{iso}= −149.5 and −147.9 ppm, respectively).[9] These contributions disappear during the annealing process (inset in Figure 7), thus confirming the previous assignment. The ^{19}F MAS NMR spectrum of the sample annealed at 773 K is reconstructed with three resonances (shown in Supporting Information). The lowest δ_{iso} values may be related to bridging fluorine atoms in AlF_6 octahedra, and the highest δ_{iso} value may be related to bridging fluorine atoms in $AlF_{6-x}(H_2O)_x$ octahedra. This confirms the occurrence of residual H_2O molecules in the sample annealed at 773 K.

The characteristic tail of the central transition of the 7 T ^{27}Al MAS NMR spectrum (see Supporting Information) and the featureless full spinning sideband manifold of the 7 and 17.6 T ^{27}Al NMR spectra of $Al_{0.82}\square_{0.18}F_{2.46}(H_2O)_{0.54}$ indicate a distribution of quadrupolar coupling constants. This is in agreement with a distribution of aluminum environments due to the occupancy of the 3d sites by both F^- ions and H_2O molecules, the disorder of the F/H_2O site, and the occurrence of cationic vacancies. The central transition of the ^{27}Al MAS NMR spectra of the hydrate form and the annealed compound recorded at 17.6 T are displayed in Figure 8a. Several contributions are distinguished for $Al_{0.82}\square_{0.18}F_{2.46}(H_2O)_{0.54}$. A way to increase resolution is to construct a two-dimensional one pulse TOP[22−24] spectrum from a conventional 1D MAS spectrum. The TOP spectrum shows the narrowing of the inner satellite transition line width and allows distinguishing four contributions (Figure 8b). Then, the ^{27}Al MAS NMR spectrum of the hydrate form has been reconstructed using four signals located at −17.9, −14.4, −11.7, and −9.4 ppm (Figure 8a, Table 4). The ^{27}Al isotropic chemical shift is sensitive to the anionic environment. The occurrence of fluorine in the vicinity of aluminum shifts the δ_{iso} to lower values.[2,3,9,11,34,35,37−42] In previous studies, lines with δ_{iso} ranging from −16 to 2 ppm were assigned to the different $AlF_{6-x}(OH)_x$ species existing in β-$AlF_{2.6}(OH)_{0.4}$ ($x < 4$)[2] and pyrochlore $AlF_{1.7}(OH)_{1.3} \cdot 0.3H_2O$ ($x < 6$),[3] the δ_{iso} value increasing with x. By analogy, $AlF_{6-x}(H_2O)_x$ species are expected to occur in $Al_{0.82}\square_{0.18}F_{2.46}(H_2O)_{0.54}$. The two lowest chemical shifts can be assigned to $AlF_4(H_2O)_2$ (−11.7 ppm) and $AlF_3(H_2O)_3$ (−9.4 ppm). These species are assumed to be metastable since these configurations led to strong electron deficiencies. It can be remembered that aging the sample led to the appearance of the pyrochlore-type structure as an impurity. Such a structure mostly contains $AlF_3(OH)_3$ species as revealed by NMR investigation.[3] It can be assumed that the water molecules contained in $AlF_4(H_2O)_2$ and $AlF_3(H_2O)_3$ species can be dissociated giving rise to hydroxyl-fluorinated species, thus forming the pyrochlore type-structure. The resonances at δ_{iso}=−14.4 and −17.9 ppm are assigned to $AlF_5(H_2O)$ and AlF_6, respectively. The disorder around Al^{3+} ions is clearly evidenced by the $\nu_{Q\eta}$ values of the four resonances which are different from zero when the 1a site symmetry is $m\bar{3}m$. One can notice that the $\nu_{Q\eta}$ value of line 1, assigned to AlF_6 species, is higher than that of α-AlF_3 (32 kHz)[43] and is of the same order of magnitude than that of β-AlF_3 (132 kHz).[11] The $\nu_{Q\eta}$ values increase from line 1 to 4, that is, with the amount of H_2O molecules around Al^{3+} ions. The proportions of the $AlF_{6-x}(H_2O)_x$ species differ from their probability of occurrence calculated based on a random H_2O/F distribution on 3d sites (Table 5) because of the presence of Al^{3+} vacancies stabilized in the ReO_3 network. Proportions of F^- ions and H_2O molecules around Al^{3+} ions can be determined from experimental ^{27}Al NMR line intensities (Table 4) and lead to the formula $AlF_{2.71}(H_2O)_{0.29}$. Taking into account the occupancy of Al^{3+} ion on the 1a site, that is, the amount of cationic vacancy and the compound formula, $Al_{0.82}\square_{0.18}F_{2.46}(H_2O)_{0.54}$, the amount of F^- ions and H_2O molecules, we obtain the formula $Al_{0.82}F_{2.22}(H_2O)_{0.24}\square_{0.18}F_{0.24}(H_2O)_{0.30}$ which gives independent insights of both the Al^{3+} ions and vacancies environments. This indicates that F^- ions prefer sitting between two Al^{3+} ions rather than between one Al^{3+} ion and one vacancy. However, around 10% of F^- ions still sit in the vicinity of a vacancy, which is in agreement with the proportion of nonbridging F^- ions in $AlF_{6-x}(H_2O)_x$ octahedra determined

(34) Chupas, P. J.; Corbin, D. R.; Rao, V. N. M.; Hanson, J. C.; Grey, C. P. *J. Phys. Chem. B* **2003**, *107*, 8327.
(35) Taulelle, F.; Pruski, M.; Amoureux, J. P.; Lang, D.; Bailly, A.; Huguenard, C.; Haouas, M.; Gérardin, C.; Loiseau, T.; Férey, G. *J. Am. Chem. Soc.* **1999**, *121*, 12148.
(36) Simon, N.; Guillou, N.; Loiseau, T.; Taulelle, F.; Férey, G. *J. Solid State Chem.* **1999**, *147*, 92.
(37) Fischer, L.; Harlé, V.; Kasztelan, S.; d'Espinose de la Caillerie, J.-B. *Solid State Nucl. Magn. Reson.* **2000**, *16*, 85.
(38) Dumas, E.; Taulelle, F.; Férey, G. *Solid State Sci.* **2001**, *3*, 613.
(39) Zhou, B.; Sherriff, B. L.; Taulelle, F.; Wu, G. *Can. Mineral.* **2003**, *1*, 891.
(40) Chupas, P. J.; Grey, C. P. *J. Catal.* **2004**, *224*, 69.
(41) Zhou, B.; Sherriff, B. L.; Hartman, J. S.; Wu, G. *Am. Mineral.* **2007**, *92*, 34.
(42) Scheurell, K.; Scholz, G.; Kemnitz, E. *J. Solid. State Chem.* **2007**, *180*, 749.
(43) Silly, G.; Legein, C.; Buzaré, J.-Y.; Calvayrac, F. *Solid State Nucl. Magn. Reson.* **2004**, *25*, 241.

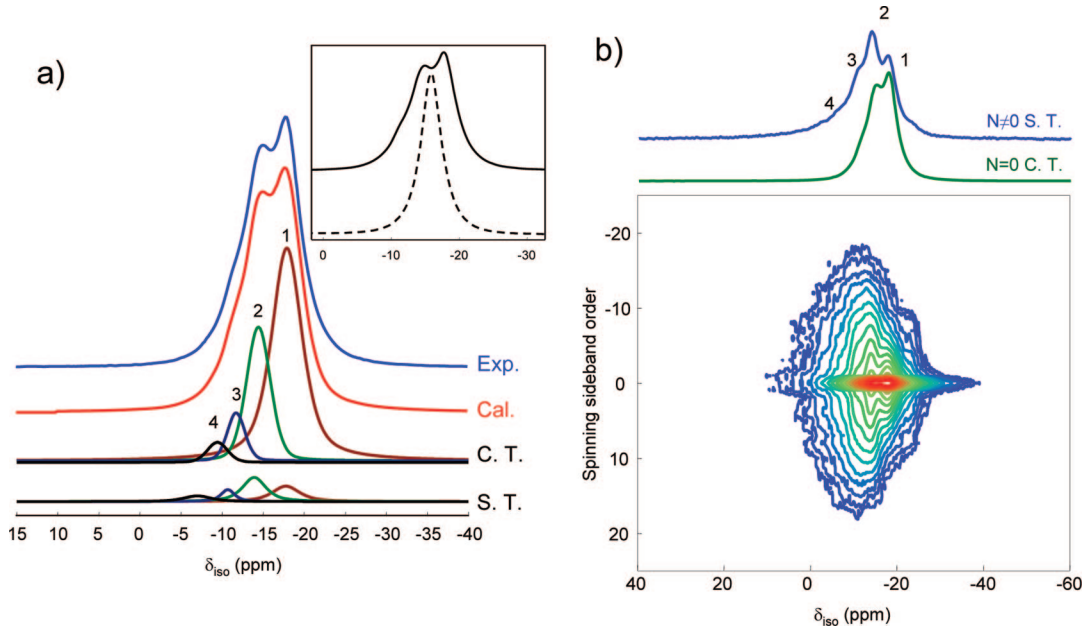

Figure 8. (a) Experimental and calculated central transitions of the ^{27}Al MAS (30 kHz) NMR spectrum of $Al_{0.82}\square_{0.18}F_{2.46}(H_2O)_{0.54}$ recorded at 17.6 T. The fitting, achieved using four contributions, takes into account the $N = 0$ band of both the satellite transitions (S.T.) ⟨3/2⟩ and the central transition (C.T.) ⟨1/2⟩. Experimental central transitions of the ^{27}Al MAS (30 kHz) NMR spectrum of $Al_{0.82}\square_{0.18}F_{2.46}(H_2O)_{0.54}$ and compound obtained after annealing at 773 K during 24 h under Ar (dash line) are presented in the inset. (b) 2D TOP spectrum of $Al_{0.82}\square_{0.18}F_{2.46}(H_2O)_{0.54}$. The $N = 0$ cross section shows the central transition spectrum, and the $N \neq 0$ sum is the satellite transition spectrum showing enhanced resolution.

Table 4. Line Label, Isotropic Chemical Shift δ_{iso} (ppm), Quadrupolar Product $\nu_{Q\eta}$ (kHz), Relative Line Intensity (%) As Deduced from the Reconstruction of the ^{27}Al MAS NMR Spectrum of $Al_{0.82}\square_{0.18}F_{2.46}(H_2O)_{0.54}$, Line Assignment, and Amount of F^- Ions and H_2O Molecules around Aluminum ions

					amount of F^- and H_2O	
line	δ_{iso} (±0.5)	$\nu_{Q\eta}$ (±10)	intensity (±0.5)	assignment	F^-	H_2O
1	−17.9	120	59.1	AlF_6	1.773	0
2	−14.4	250	28.7	$AlF_5(H_2O)$	0.717	0.143
3	−11.7	360	7.8	$AlF_4(H_2O)_2$	0.156	0.078
4	−9.4	560	4.4	$AlF_3(H_2O)_3$	0.066	0.066
					$AlF_{2.71}(H_2O)_{0.29}$	

Table 5. Probability of Occurrence of the $AlF_{6-x}(H_2O)_x$ Species Based on a Random H_2O/F Distribution on 3d Sites

AlF_6	$AlF_5(H_2O)$	$AlF_4(H_2O)_2$	$AlF_3(H_2O)_3$	$AlF_2(H_2O)_4$	$AlF(H_2O)_5$	$Al(H_2O)_6$
30.4	40.0	22.0	6.4	1.1	0.1	/

from ^{19}F NMR (∼12%, Table 2). The occurrence of water molecule between two Al^{3+} ions can be excluded because of unrealistic electronic configuration. The larger amount of H_2O molecules around cationic vacancies than around Al^{3+} ions reinforces this assumption. Moreover, some water molecules are located between two vacancies, in agreement with the high vacancy content, that is, 18%. These water molecules are stabilized by hydrogen bonding. The departure of such water molecules matches with the second weak departure observed in the IC curve $m/z = 18$ occurring at 563 K (Figure 3).

Finally, the annealing process at 773 K leads to a compound in which the ^{27}Al resonances at $\delta_{iso} = -9.4$ and -11.7 ppm have disappeared confirming the previous assignments of the hydrated species. For this compound, a single ^{27}Al NMR signal is detected (Figure 8a and Supporting Information) and reconstructed (see Supporting Information) using the following parameters: $\delta_{iso} = -15.9$ (±0.2) ppm and $\nu_{Q\eta} = 140$ (±20) kHz. The δ_{iso} value is intermediate between those assigned to AlF_6 and $AlF_5(H_2O)$ species in $Al_{0.82}\square_{0.18}F_{2.46}(H_2O)_{0.54}$ before annealing and close to the δ_{iso} value of the line assigned to AlF_6 and $AlF_5(OH)$ species in β-$AlF_{2.6}(OH)_{0.4}$.[2] The quadrupolar product $\nu_{Q\eta}$ value is significantly larger than that in α-AlF_3 ($\nu_{Q\eta} = 32$ kHz).[43] This may be related to a larger disorder around Al^{3+} ions in $Al_{0.82}\square_{0.18}F_{2.46}(H_2O)_{0.54}$ after annealing at 773 K than in α-AlF_3. Finally the ^{27}Al NMR parameters confirm the IR and ^{1}H and ^{19}F NMR observations, that is, the occurrence of residual H_2O molecules in the sample annealed at 773 K.

On the basis of the above results, a representation of the structure of $Al_{0.82}\square_{0.18}F_{2.46}(H_2O)_{0.54}$ can be proposed with a view of the cubic unit cell with the occurrence of one vacancy where a 2:1 (X···H−O−H···X) complex occurs (Figure 9A) and a view of a super cell showing two vacancies located side by side with an isolated water molecule in between (Figure 9B).

3. Acidic Properties. The acidic properties of this new aluminum fluoride hydrate have been characterized by adsorption of probe molecules (CO and pyridine) followed by FTIR spectroscopy. The use of two different probes enables a better description of the surface properties. As a weak base, CO enables the detection of Brønsted and Lewis acidities, and the adsorption of small doses enables the detection of the strongest sites.[44] The pyridine molecule is a strong base and is commonly used to probe Lewis acidity and characterize strong Brønsted acidic sites.

Prior to the characterization of the surface, the material is activated to remove surface impurities. The activation is carried out at 573 K under vacuum.[32] In addition, the specific

(44) Hadjiivanov, K. I.; Vayssilov, G. N. *Adv. Catal.* **2002**, *47*, 307.

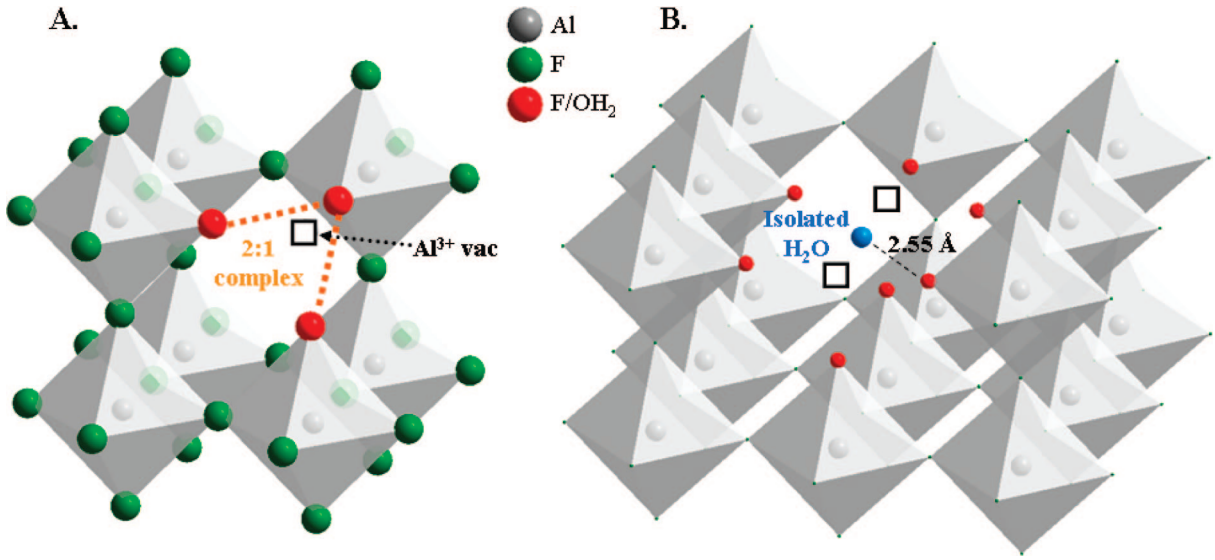

Figure 9. Schematic representation of the structure. (A) View of the cubic unit cell with the occurrence of one Al^{3+} vacancy with a 2:1 complex. (B) View of the structure with the occurrence of two vacancies located side by side with an isolated water molecule in between.

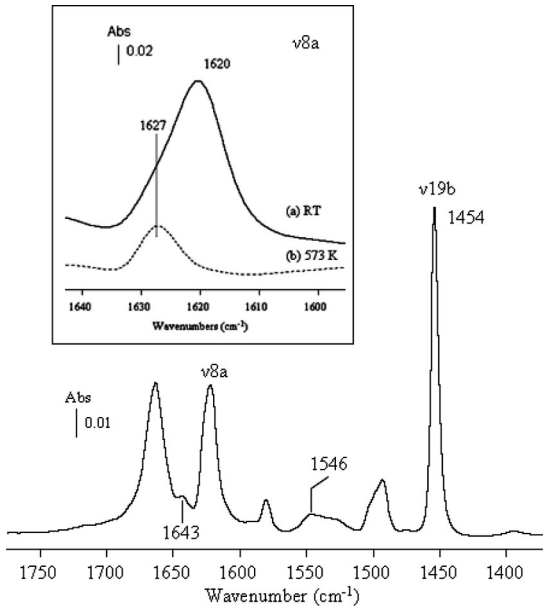

Figure 10. IR difference spectrum of adsorbed pyridine (133 Pa) after activation at 573 K and recorded after evacuation at room temperature. Inset: extension on the ν8a vibration mode from IR spectra recorded at (a) RT and (b) after thermodesorption at 573 K.

surface area of the sample annealed overnight at 573 K is 61 $m^2 \cdot g^{-1}$ suitable for FTIR characterization. The material is then characterized using a pyridine molecule and CO adsorption performed at low temperature (100 K). In a second step, the surface is further activated successively at 673 and 773 K to investigate by using CO adsorption the effect of the dehydration on the acidic properties.

Activation at 573 K. After activation at 573 K, 133 Pa of pyridine are adsorbed at room temperature. Physisorbed species were removed by evacuation under secondary vacuum at RT. The spectrum showing the vibration modes (1400−1700 cm^{-1}) of coordinated pyridine molecule is displayed in Figure 10. Note that the band located at 1660 cm^{-1} is ascribed to the bending mode of the water molecule which is slightly shifted after pyridine adsorption. Both Lewis and Brønsted acidities are detected. The protonation of the pyridine molecule is clearly evidenced by the bands observed at 1546 and 1643 cm^{-1}, ascribed to pyridinium species. The bands detected at 1620 and 1454 cm^{-1} are related to the ν8a and ν19b modes of coordinated pyridine which characterize the Lewis acidity. Their positions account for the strength of the Lewis acidity, that is, the higher the wavenumber, the stronger the acidity. The ν8a band which is more sensitive to the Lewis strength presents a shoulder (inset Figure 10) detected at higher wavenumber, that is, 1627 cm^{-1}, revealing the occurrence of strong Lewis acid sites. The strength of such a site has been ascertained by thermodesorption at 573 K (inset Figure 10) showing the disappearance of the lowest component at 1620 cm^{-1} whereas the contribution at 1627 cm^{-1} remains. It should be noted that same values have been reported for β-AlF_3,[32] highlighting the Lewis acidic character of this new material. Then, pyridine adsorption clearly proves the occurrence of accessible Lewis as well as strong Brønsted sites.

Effect of Annealing upon the Acidic Properties. After annealing at 573 K, the material still contains a lot of water molecules (Figure 5) associated with cationic vacancies. To get more insight into the origin of the acidic properties of the solid, the effect of dehydration upon the acidic properties has been investigated by using CO adsorption. The use of such a molecule enables a more fine description of the surface, the CO stretching mode lying from 2150 to 2240 cm^{-1}. IR spectra of saturated CO adsorbed after annealing treatment performed at 573, 673, and 773 K are displayed in Figure 11. Different regions can be distinguished: (i) ν(CO) > 2200 cm^{-1} accounts for strong Lewis acid sites, (ii) bands located between 2200−2180 cm^{-1} account for medium Lewis acid sites, and (iii) the region lying from 2180 to 2150 cm^{-1} are ascribed either to Brønsted or weak Lewis acid sites. Finally, physisorbed species are detected for ν(CO) < 2150 cm^{-1}. The dehydration process induces a drastic change of the surface structure as revealed by the evolution ν(CO) position. At first, the bands located at ν(CO) > 2200 cm^{-1} decrease upon annealing. This is going with an increase of the bands lying between 2180−2195 cm^{-1} related to

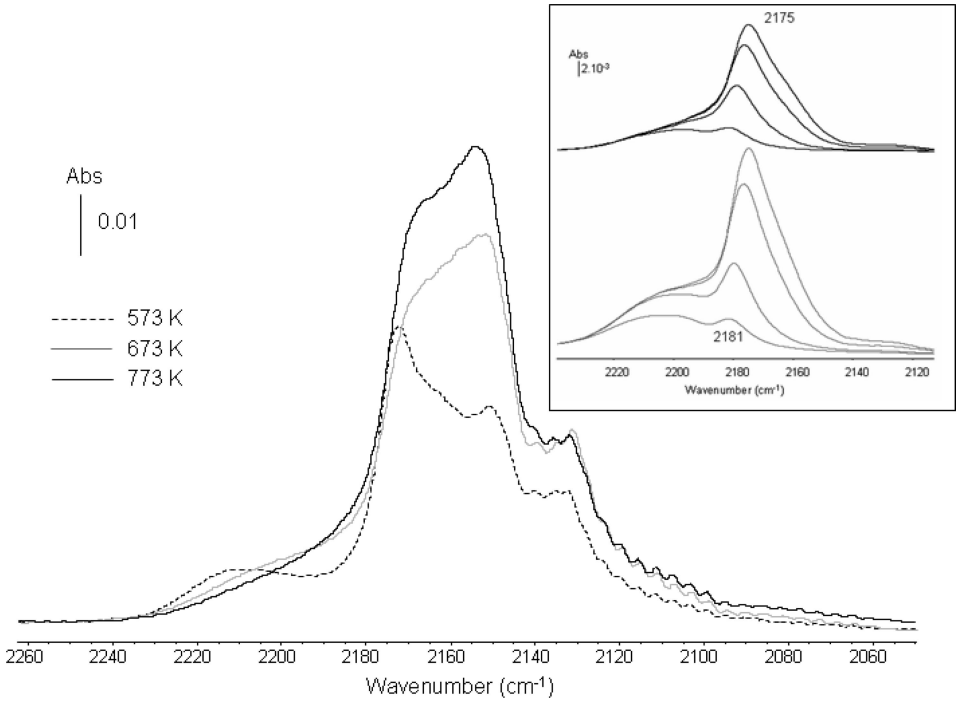

Figure 11. IR difference spectra of adsorbed CO on aluminum fluoride hydrate activated at various temperatures overnight. Inset: Detailed analysis for samples activated at 673 (down) and 773 K (top) after successive (4) additions of CO doses.

medium Lewis acidic sites. Additionally, a band located at around 2160−2165 cm^{-1} strongly increases upon annealing which proves the Lewis origin of this band. Thermal treatments clearly convert the strong Lewis acid sites (ν(CO) > 2200 cm^{-1}) into medium (2180−2200 cm^{-1}) and weak (2160−2165 cm^{-1}) ones. After the annealing treatment at 773 K, the solid is closely related to the rhombohedral form of α-AlF_3 (Figure 4). CO adsorption performed after such a treatment revealed the occurrence of weak and medium Lewis acidity which is in good agreement with the modeled acidic behavior for the (0001) α-AlF_3 surface.[12,13] Since dehydration led to the conversion of the strong Lewis acid sites into weaker ones, it can be assumed that the occurrence of water molecules and cationic vacancies perturbed the surface structure, generating accessible and strong Lewis acidic sites.

A detailed analysis using small amounts of CO evidence the occurrence of Brønsted sites through ν(CO) bands lying between 2181 and 2175 cm^{-1}. The relevant point here is the stability of the Brønsted sites upon annealing treatments since Brønsted contribution is still present after treatments at 673 and 773 K (inset of Figure 11). Obviously, the amount of Brønsted sites decreases upon annealing as revealed by the ν(CO) intensities. The ν(CO) positions as well as the detection of pyridinium species account for the presence of strong Brønsted acid sites which can be ascribed to surface water molecules. Such a result confirms that water molecules can act as a strong Brønsted site.[6]

Finally, it was interesting to estimate the relative contribution between Lewis and Brønsted acidities. In this aim, ν(CO) bands related to each contribution have been integrated. An extension coefficient equal to 2.1 and 2.7 $cm \cdot \mu mol^{-1}$ for ν(CO) > 2200 cm^{-1} and ν(CO) < 2200 cm^{-1}, respectively, have been used. Calculation has been achieved for CO adsorption performed after activation at 573 K which can be considered as a suitable temperature for catalytic reactions. The estimation leads to 0.544 Lewis acid sites and 0.504 Brønsted sites per squared nanometer. Therefore, the surface exhibits an equivalent number of Brønsted and Lewis acid sites which defines this new material as bifunctional. Specific reactions could be achieved to confirm such behavior.

Conclusion

A new aluminum fluoride hydrate was prepared using microwave-assisted synthesis. The acidification of the medium using high HF contents favors the stabilization of water molecules in the first coordination sphere of the cation, as opposed to OH groups previously described in the pyrochlore and HTB compounds. The variation of the charge density upon the octahedra induced by the substitution of F^- ions by H_2O molecules is balanced by the occurrence of cationic vacancies, as revealed by the Rietveld refinement. This is the first example of aluminum vacancy compound in the Al-based fluorides system. ^{19}F NMR investigations confirm the occurrence of cationic vacancies through the identification of bridging and nonbridging F^- ions. $AlF_{6-x}(H_2O)_x$ species containing various numbers of water molecules were quantified using high field ^{27}Al NMR spectroscopy. This quantification led to the formula $Al_{0.82}F_{2.22}(H_2O)_{0.24}\square_{0.18}F_{0.24}$-$(H_2O)_{0.30}$ which gives independent insights of both the Al^{3+} ions and vacancy environments and shows the occurrence of unusual H_2O molecules surrounded by two cationic vacancies. Hydrogen-bond interactions contribute to stabilize the cationic vacancies. FTIR spectroscopy enables the characterization of a 2:1 complex (X···H−O−H···X where X is a proton acceptor) formed by water molecules, which is stable up to 773 K. The cubic symmetry is transformed

upon annealing into a rhombohedral form at around 573 K, that is, after the departure of isolated water molecules.

The investigation of the acidic properties evidences various acidic behaviors depending on the activation temperature. At 573 K, both strong Lewis and Brønsted acidic sites are present at the surface. Such a configuration can be used for reactions involving the synergy between Lewis/Brønsted acidities. By contrast with the modeled α-AlF_3 phase, the strong Lewis acidity occurring at this temperature has been rationalized by the presence of water/Al^{3+} vacancy inducing a peculiar surface structure. Further dehydration leads to a conversion of strong Lewis acid sites into weaker ones, and the obtained surface structure resembles that modeled for the (001) surface of α-AlF_3.

Acknowledgment. The EU is acknowledged for financial support through the 6th Framework Program (FUNFLUOS, Contract No. NMP3-CT-2004-5005575). Lydia Raison is gratefully acknowledged for performing EMPA analysis.

Supporting Information Available: ^{1}H MAS (30 kHz) NMR spectrum, ^{19}F MAS (30 kHz) NMR experimental and calculated spectra of $Al_{0.82}\square_{0.18}F_{2.46}(H_2O)_{0.54}$ after annealing at 773 K during 24 h under Ar, isotropic chemical shifts δ_{iso} (ppm), line widths (ppm) and relative intensities (%) as deduced from the reconstruction of the ^{19}F NMR spectrum of $Al_{0.82}\square_{0.18}F_{2.46}(H_2O)_{0.54}$ after annealing at 773 K during 24 h under Ar, ^{27}Al MAS (30 kHz) one pulse NMR spectrum recorded at 17.6 T of $Al_{0.82}\square_{0.18}F_{2.46}(H_2O)_{0.54}$ and $Al_{0.82}\square_{0.18}F_{2.46}(H_2O)_{0.54}$ after annealing at 773 K during 24 h under Ar, ^{27}Al MAS (25 kHz) one pulse NMR spectrum of $Al_{0.82}\square_{0.18}F_{2.46}(H_2O)_{0.54}$ recorded at 7 T, and experimental and calculated central transitions of the ^{27}Al MAS (30 kHz) NMR spectrum recorded at 17.6 T of $Al_{0.82}\square_{0.18}F_{2.46}(H_2O)_{0.54}$ after annealing at 773 K during 24 h under Ar (PDF). This material is available free of charge via the Internet at http://pubs.acs.org.

CM8023617